Optics and Lasers in Engineering 152 (2022) 106972

Contents lists available at ScienceDirect

Optics and Lasers in Engineering

journal homepage: www.elsevier.com/locate/optlaseng

Anamorphic beam shaping system designed to optimize irradiance distribution in the Cofiblas process for glass nanofibers production

Joaquín Penide[a], Félix Quintero[a,b,*], José Luis Fernández[b], Mónica Fernández-Arias[a,b], Raúl Barciela[a,b], Jesús del Val[a,c], Fernando Lusquiños[a,b], Juan Pou[a,b]

[a] CINTECX, Universidade de Vigo, LaserON Research Group, 36310, Vigo, España
[b] Applied Physics Department, Universidade de Vigo, E.E.I., 36310, Vigo, España
[c] Centro Universitario de la Defensa, Escuela Naval Militar, Plaza de España 2, 36920 Marín, España

ARTICLE INFO

Keywords:
Anamorphic optics
Laser beam shaping
Glass nanofibers
Laser glass processing
Cofiblas

ABSTRACT

Glass fibers play a key role as reinforcements in composite materials, where increasing mechanical properties at affordable costs are required in applications such aerospace, automotive and wind turbine manufacturing. The production of glass nanofibers augurs a substantial enhancement of their performance. However, although different techniques are currently used to produce glass, polymer or carbon nanofibers, none of them is practical to continuously produce solid, non-porous and separated glass nanofibers with capability to feasibly scaling up for mass production. The continuous fiberizing by laser melting (Cofiblas), makes possible to obtain ultrafine fibers with virtually infinite length.

Here, we provide a deep analysis on the influence of the laser beam shaping system on the performance of the Cofiblas technique. Two different optical systems are compared: the first one consists of a beam-splitter coupled to a set of mirrors and spherical lenses. While the second one, is based on an anamorphic system comprising a simple combination of cylindrical and spherical lenses. Both configurations are evaluated and compared in several sets of experiments with the main target of obtaining continuous glass nanofibers with the smallest diameter. The anamorphic system generates an elliptical Gaussian distribution of the laser beam irradiance, which increases the energy absorbed by the preform. As a result, continuous silica nanofibers with diameters 84.5% smaller are obtained with the anamorphic system, compared with the optical system constituted by spherical lenses.

1. Introduction

The development of new materials with improved properties and better performance on service is a stimulating field of research for scientists and engineers. A notable category in the scope of new materials is occupied by the nanofibers and nanowires. A wealth of works on the synthesis and properties of nanofibers and nanowires explored their applications in many different fields. Among this variety of applications, the search for better mechanical features and lightweight materials are likely the most requested ones in the industry to improve the performance of structural elements and energy efficiency. With this objective, nanofibers and nanowires have been pointed out as reinforcement for potentially high-performance composites. Nanofiber reinforced composites have shown an improvement in their mechanical behavior, nevertheless, the use of short discontinuous fibers or the inadequate alignment of this reinforcements could mean that those mechanical properties do not improve as much as expected [1]. In addition to an adequate length and alignment, strength and toughness have been also highlighted as critical features for nanofibers in reinforced composites [2]. As is known, both strength and toughness increase significantly for decreasing diameters [3,4].

Glass fibers occupy a prominent place in the fiber-reinforced composites market [5], where their good mechanical properties and optimal photochemical durability at affordable costs are required in applications such as aerospace, automotive and wind turbine manufacturing [6]. The sustainable mass production of glass nanofibers augurs a substantial enhancement of their applications thanks to a substantial enhancement of their mechanical properties. Recent works in very short and thin silica nanofibers demonstrated outstanding tensile strength and ductility, exceeding the typical properties of glass fibers by a factor of [5,7]. Features of these high-performance nanofibers depend on the precursor material, but they are also highly influenced by the manufacturing process [7,8]. The techniques usually employed to produce glass nanofibers involve melting and subsequent stretching of the precursor material. Conven-

Abbreviations: BSS, Beam Shaping System; DoE, Design of experiments; SEM, Scanning electron microscope.

* Corresponding author.
E-mail address: fquintero@uvigo.es (F. Quintero).

https://doi.org/10.1016/j.optlaseng.2022.106972
Received 10 September 2021; Received in revised form 10 January 2022; Accepted 19 January 2022

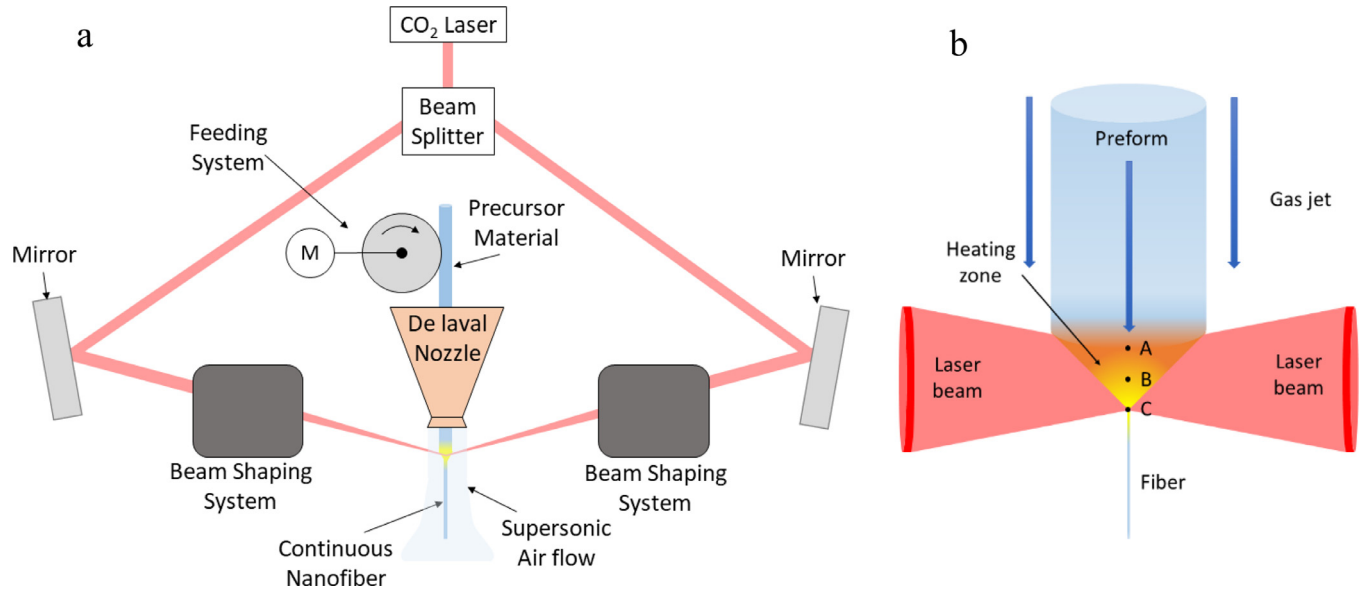

Fig. 1. (a) Experimental setup showing the geometrical configuration of both symmetric laser beams directed to the glass preform going out of the de Laval nozzle. (b) Detail of the irradiated zone on the preform.

tional techniques to produce continuous glass fibers, such as melt spinning, rely on the mechanical drawing of the filament by a reel from the bushing tip or from the molten preform. However, conventional melt spinning processes are not able to produce fibers thinner than about 2 μm [8].

Laser spinning has demonstrated to be a feasible technique to produce long nanofibers of ceramic materials with different compositions [9–11]. However, this process is not continuous and, consequently, the resulting nanofibers present non-customizable lengths and diameters. More recently, glass nanofibers with exceptional small diameter and virtually unlimited length were obtained by the authors using the new continuous laser supersonic fiberizing (Cofiblas) technique [12]. In addition, the diameter of the obtained fibers can be precisely controlled, producing nonporous, solid and free-standing separated nanofibers. All these properties make possible for the nanofibers to be woven, which could be very useful in the development of innovative fiber-based high-performance materials. This unprecedented process combines a high-power laser with a supersonic gas jet to reduce the diameter of a glass preform. Fig. 1.a presents an scheme of the experimental set-up to run the Cofiblas process. Specifically, it employs a high power CO_2 laser and a beam-splitter that divides the continuous emission into two identical laser beams. Both laser beams are redirected by several mirrors through the Beam Shaping System (BSS) and oriented so as they face each other on the precursor material.

The most important achievements of this technique are the quick heating, stretching and cooling of the preform, which all together lead to the high stability in continuous operation, which in turn makes possible that these fibers are virtually endless. The high energy delivered by the laser leads to extreme temperature gradients, thus the Cofiblas process is able to elongate the preform at extremely high strain rates, reducing its diameter from several tenths of millimeter into a nanofiber in some milliseconds. The supersonic gas jet produces a distributed stretching force around and along the molten material. The axial distribution of the elongational forces is essential for the stability of the process, since it allows to reach a large axial stress and strain ratios at the sections where the filament is molten, and, conversely, very low stress where the nanofiber is solid and can't withstand the high tensile force required to stretch the molten filament [12].

A precise heating and cooling of the filament is also crucial. The use of two laser beams guarantees an uniform distribution of the energy on the preform. Also, a precise control of the irradiance along the stretching zone is required to keep the stability of the molten filament. The glass preform must be heated to a temperature range corresponding to a suitable viscosity window for the elongation process, called the fiber forming viscosity [8,11]. A high irradiance peak could lead to excessive filament temperature and the viscosity drops below the lower limit, which disturbs the stability of the process and causes the fiber breakage. On the contrary, a reduced irradiance leads to a low temperature, exceeding the upper viscosity limit, and, consequently, the tensile force exerted by the gas flow is not able to stretch the molten material, resulting in a thick fiber. Additionally, the irradiance profile must be adapted to the reduction of diameter of the filament, since the energy absorbed by the preform at the beginning of the process is high enough to initiate its elongation with moderately high irradiance (zone A in Fig. 1.b). However, as the diameter of the filament decreases, so does the absorbed energy, just because the irradiated volume is getting smaller (zone B in Fig. 1.b). Then, the laser beam may not be able to supply the necessary radiant power to the filament to keep the viscosity in the proper range. When this occurs, then the elongation of the fiber ends prematurely and the process fails (zone C in Fig. 1.b). Consequently, a precise control of the irradiance distribution along the filament is required. For this reason, the adequate design of the BSS is crucial for the proper functioning of the process, since it allows to obtain an adequate distribution of irradiance along the axis of the filament and a precise control thereof.

The present paper, provides a deep analysis on the influence of the BSS employed to adjust the irradiance profile on the filament in the Cofiblas technique, designed to increase the stability of the process and give a continuous nanofiber. With this aim, we explain the design of two different configurations of the BSS, compare their results in a series of experiments to produce glass nanofibers, and, finally, we analyze the factors affecting their performance.

2. Materials and methods

The experimental set-up comprises a high-power CO_2 laser (Rofin DC-035) emitting a maximum output radiant power of 3.5 kW with a beam transverse mode very close to TEM_{00} ($M^2 \leq 1.05$), operated in continuous regime and wavelength $\lambda = 10.6$ μm. The optical system, includes a beam splitter together with two symmetric mirrors and two beam shaping systems (BSS), see Fig. 1.a. First, the laser beam is divided

Table 1
Ranges of parameters evaluated with the spherical lenses.

Laser beam	Radiant flux, Φ_e (W)	213 – 1750
Spherical lens	Focal distance, f (mm)	710
	Working distance, *WD* (mm)	1000 – 1150
	Beam diameter at *WD*, $2\omega_{is}$ (mm)	8.2 – 12.4
Gas	Gas pressure, p (bar)	3.5
Preform	Preform diameter, D_i (μm)	600
	Feeding speed, v (μm•s^{-1})	0.01 – 5

into two by means of a beam splitter 50/50 (Rofin EBS). The beam splitter includes a diamond window which reflects 50 % of the beam with the same original beam profile, the remaining 50 % pass through the diamond window with an accuracy of < 1 % between both laser beams. Each beam is redirected by a plane copper mirror to hit the preform at the outlet of the nozzle. With regard to each beam-shaping system, two different configurations were analyzed. The first one, was constituted by a spherical lens with long focal length. The second one, is based on the combination of a cylindrical lens and a spherical lens.

Pure silica fibers (CeramOptec, Germany) with 600 μm of diameter were employed as the precursor material in all experiments. The process gas employed was compressed air supplied at a pressure of 350 kPa to the de Laval nozzle, which generates a supersonic gas jet to stretch the molten filament. The morphology of the fibers was characterized using a field-emission SEM (JEOL JSM-6700F), as-produced fibers were deposited on carbon adhesive discs for SEM imaging and their diameters were measured in the calibrated micrographs. A minimum of five fibers were measured in a single experiment, but the typical number of samples was around fifteen.

2.1. Set of experiments with the BSS-1 of spherical lenses

In the first configuration tested (BSS-1), the beam shaping system is formed by a single ZnSe plano-convex spherical lens with focal length $f = 710$ mm which is used to focus the laser beam on the preform. This long focal length and large depth of focus makes possible to keep the irradiance of the laser beam on the interaction zone very stable, despite possible vibrations of the preform. Subsequently, an extensive set of experiments were performed by modifying parameters such as radiant flux, beam diameter at the incident plane (central plane of the preform), $2\omega_{is}$, which is adjusted by changing the lens distance to the incident plane (working distance, *WD*), and the feeding speed of the preform into the process nozzle. Table 1, shows the corresponding ranges of values for each parameter used throughout this set of experiments. The beam diameters and feeding speed of the preform were set for each trial, while the radiant power was adjusted independently at each trial to the maximum that ensures the production of continuous fibers.

2.2. Design and calculations of the BSS-2 with cylindrical and spherical lenses

In this set-up a new beam shaping system, BSS-2, based on an anamorphic optical system was designed with the purpose of optimizing the irradiance distribution of the laser beam along the filament axis (*y*-axis in Fig. 2). Different anamorphic configurations comprising lenses, mirrors, and/or prims are available for different purposes [13,14]. In our case, the goal of the anamorphic system is simply to reshape and focus a collimated high-power laser beam, so a combination of a spherical lens with a cylindrical lens was chosen because this configuration provides appropriate beam quality while maintaining simplicity, a small number of optical surfaces, ruggedness and low cost.

An analytical calculation of the Gaussian beam propagation through the optical system for different combinations of spherical and cylindrical lenses (either convergent or divergent) was carried out to select the proper lens combination. In this analysis, we assume that the cylindrical lens transforms the original circular Gaussian beam into an elliptic Gaussian beam [15] which exhibits simple (or orthogonal) astigmatism: the light spot is elliptical with the same orientation in every beam cross section, so there are two principal meridional planes, perpendicular to each other, which contain the propagation axis of the beam and the major or minor axis of the ellipses of constant irradiance. The irradiance profile varies as the beam propagates through space, its expression in a Cartesian coordinate system can be derived from the equation of the electric field [15] as:

$$I(x,\ y,z) = I_0 \frac{\omega_{0x}\omega_{0y}}{\omega_x(z)\omega_y(z)} \exp\left[-2\left(\frac{(x-x_c)^2}{\omega_x^2(z)} + \frac{(y-y_c)^2}{\omega_y^2(z)}\right)\right] = I_0(z)\exp\left[-2\left(\frac{(x-x_c)^2}{\omega_x^2(z)} + \frac{(y-y_c)^2}{\omega_y^2(z)}\right)\right] \quad (1)$$

where the z-axis is parallel to the direction of propagation, I_0 is a constant, $I_0(z)$ is the irradiance at the center of the beam cross section at an arbitrary z position, $x - x_c$ and $y - y_c$ are the distances from the propagation axis of the beam on the principal meridional planes, $\omega_x(z)$ and $\omega_y(z)$ are the respective Gaussian beam radii, where the irradiance is $1/e^2$ (13.5 %) of $I_0(z)$, and ω_{0x} and ω_{0y} are the Gaussian beam radii at the respective waists, which occur at different z values. If we choose the z axis to coincide with the propagation axis of the beam, then $x_c = y_c = 0$. The value of $I_0(z)$ can be related to the total radiant flux (or radiant power) of the laser beam, Φ_e, by integrating the irradiance over the cross section:

$$\Phi_e = \int\int_{-\infty}^{\infty} I_0(z)\exp\left[-2\left(\frac{(x-x_c)^2}{\omega_x{}^2(z)} + \frac{(y-y_c)^2}{\omega_y{}^2(z)}\right)\right]dx\,dy = (1/2)I_0(z)\,\pi\,\omega_x(z)\,\omega_y(z) = (1/2)I_0\,\pi\,\omega_{0x}\,\omega_{0y} \quad (2)$$

In order to analyze the beam propagation and to design the BSS, we employed the procedure for tracing the characteristics of a Gaussian beam through a train of lenses demonstrated by Sidney A. Self [16]. Although this method applies, in principle, only to spherical Gaussian beams, we can apply it to our case because the parameters of an elliptic Gaussian beam (with simple astigmatism) on each principal meridional plane are exactly the same as those of a spherical Gaussian beam with the same waist radius and location (i.e., the elliptical beam can be treated as two independent spherical beams [15]). Self-generalized the lens formulas of geometrical optics by considering the waist of the input beam as the object and the waist of the output beam as the image and introducing the Rayleigh range of the beam, which is modified after the passage through each lens and thus must be recalculated for each step. To solve the passage through a system of cascaded lenses, the image formed by each lens is used as the object for the next lens, in the same manner as in geometrical optics. With this procedure we can determine the critical parameters such as magnification, focal length(s), and object and image position. Then, at the design stage, we applied this procedure, detailed in the following paragraphs, to estimate the obtainable ranges of the beam radii using different combinations of commercially available lenses. As a result of this stage, we obtain a selection of the appropriate lenses to set-up the effective optical system to generate the different irradiance profiles at the incident plane. After the design stage, we used the same procedure at the experimentation stage with the purpose of obtaining the positions of the selected lenses which generate the desired irradiance profiles at the incident plane. At this plane, we characterize each irradiance profile by the beam radii on the principal meridional planes, ω_{ix} and ω_{iy}.

Fig. 2 represents the set-up of the BSS-2 that we designed together with a representation of the Gaussian beam propagation. First, the same plano-convex spherical lens as in the BSS-1 ($f_s = 710$ mm) is situated at the position z_s, while the glass preform is situated at the position z_i. Then, the plano-convex cylindrical lens with focal length $f_c = 267$ mm is situated at the position z_c with its rotation axis parallel to the x-axis. The input beam of the BSS-2 is the collimated beam emitted by the

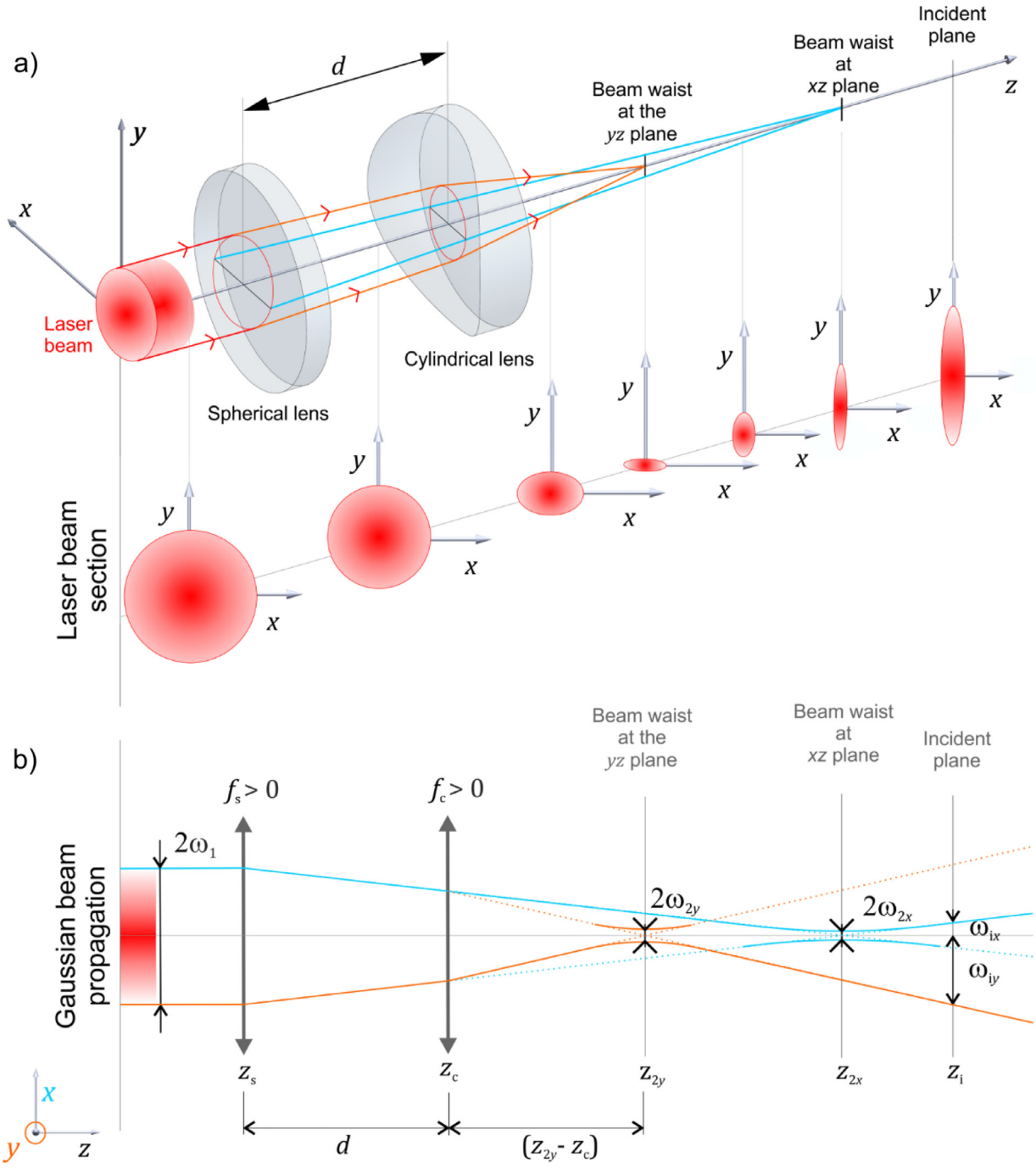

Fig. 2. (a) Scheme of the experimental setup of the BSS-2 showing a representation of the laser beam cross section along the optical path. (b) Representation of the main optical parameters of the BSS-2 employed to calculate the Gaussian beam propagation.

laser (once divided in two by means of the beam splitter) entering the spherical lens. To characterize this beam we employ its waist radius $\omega_1 \approx 10$ mm and its waist location z_1. Its Rayleigh range, z_{R_1}, is:

$$z_{R_1} = \frac{\pi\omega_1^2}{\lambda} \approx 30 \text{ m} \tag{3}$$

The lens equation for a Gaussian beam [16] is:

$$\frac{1}{s + z_R^2/(s-f)} + \frac{1}{s'} = \frac{1}{f} \tag{4}$$

where s is the object distance (distance from the input beam waist to the lens) and s' is the image distance (distance from the lens to the output beam waist). Particularizing (4) for the spherical lens, $z_R = z_{R_1}$, $f = f_s$, $s_1 = z_s - z_1$ and $s_1' = z_{2x} - z_s$. Taking into account that the waist of the beam emitted by the laser is located no far from the laser cavity (and thus no far from the spherical lens) and considering (3), we can assume that $z_{R_1} \gg s_1$. Also, from (3), we can ensure that $z_{R_1} \gg f_s$ and we can write

$$z_{R_1} \gg f_s,\ s_1 \tag{5}$$

Applying (5) to (4), we obtain that the image distance s_1' practically equals the focal length independently of the object distance s_1. The image waist radius on the principal meridional plane xz, ω_{2x}, can be ob-

tained from the formula of magnification m_s and further simplified by considering (5):

$$m_s = \frac{\omega_{2x}}{\omega_1} = \frac{1}{\left[\left(1-\frac{s_1}{f_s}\right)^2 + \left(\frac{z_{R_1}}{f_s}\right)^2\right]^{1/2}} \Rightarrow \omega_{2x} = \frac{\lambda f_s}{\pi \omega_1} \tag{6}$$

The beam radius on the *xz* meridional plane at the incident plane, ω_{ix}, placed at a distance $z_{xi} = z_i - z_{2x}$ from the beam waist ω_{2x}, can be calculated from:

$$\omega_{ix} = \omega_{2x}\left[1 + \left(\frac{z_{xi}}{z_{R_2}}\right)^2\right]^{1/2} \tag{7}$$

where the Rayleigh range for the output beam from the spherical lens is:

$$z_{R_2} = \frac{\pi \omega_{2x}^2}{\lambda} \tag{8}$$

Subsequently, consistent with the procedure for a cascaded system and the model of independent propagation of the irradiance profile in both orthogonal planes, the image waist of the spherical lens can be considered as the virtual object of the cylindrical lens in the principal meridional plane *yz*. The magnification m_c for the cylindrical lens relates the object waist, ω_{2x}, to its image in the plane *yz*, with $s_2 = -(z_{2x} - z_c)$, written for simplicity as $z_{cx} = (z_{2x} - z_c)$:

$$m_c = \frac{\omega_{2y}}{\omega_{2x}} = \frac{1}{\left[\left(1-\frac{-z_{cx}}{f_c}\right)^2 + \left(\frac{z_{R_2}}{f_c}\right)^2\right]^{1/2}} \tag{9}$$

And the image distance $s_2' = z_{2y} - z_c$, written as z_{cy}, can be obtained from Eq. (4) as:

$$\frac{1}{-z_{cx} - z_{R2}^2/(f_c + z_{cx})} + \frac{1}{z_{cy}} = \frac{1}{f_c} \tag{10}$$

Finally, the distance $z_{yi} = z_i - z_{2y}$ from the beam waist ω_{2y} for a certain beam radius, ω_{iy}, along the meridional plane *yz* at the incident plane, can be calculated from:

$$z_{yi} = \frac{\pi \omega_{2y}}{\lambda}\left(\omega_{iy}^2 - \omega_{2y}^2\right)^{1/2} \tag{11}$$

Regarding the effect of lens aberrations on the beam shaping, the optical configuration is quite insensitive because:

a) Beam propagation is paraxial in a high grade throughout the whole beam shaping system. This is because the laser beam at the input plane of the first lens has a practically pure single transversal mode ($M^2 \leq 1.05$) and is well collimated with a quite large Gaussian beam radius of 10 mm, and the employed lenses have relatively large focal lengths. The largest half angle divergence of the beam can be calculated as

$$\theta_{max} = \frac{\lambda}{\pi \omega_{2y}} = 0.043 \text{ rad} \tag{12}$$

where we have taken $\omega_{2y} = 0.078$ mm which is the minimum value obtained for the different lenses' positions employed in the experiments.

b) The beam axis nominally coincides with the optical axis of the beam shaping system, so is perpendicular to both lenses. Once well aligned the system, there are no concerns about aberrations derived from decentering or tilt, like coma.

c) The effects of spherical aberration on the degradation in the beam-quality factor, M^2, when a TEM_{00} laser beam passes through a thin lens have been described in [17]. Theory predicts that the laser beam quality should remain essentially unchanged until the incident Gaussian beam radius exceeds a critical value ω_q given by expression (27) of [17], above which the beam quality will degrade rapidly. Particularizing that expression to our optical system parameters, we found that $\omega_q = 36$ mm for a plano-convex spherical lens with a focal length of 710 mm while $\omega_q = 28$ mm for a focal length of 267 mm. Those values are substantially larger than our beam radius, so the spherical aberration is not a concern.

Table 2
DoE1.

	Levels	
Factors	1	2
Major axis, $2\omega_{iy}$ (mm)	30	45
Spot area, A ($\pi \bullet 4^{-1}$ mm^2)	90	180
Feeding speed, v (μm•s^{-1})	100	500

Table 3
DoE2.

	Levels	
Factors	1	2
Major axis, $2\omega_{iy}$ (mm)	20	30
Spot area, A ($\pi \bullet 4^{-1}$ mm^2)	40	60
Feeding speed, v (μm•s^{-1})	1	4

2.3. Experiments with the BSS-2

Due to the wide number of factors involved, we used the design of experiments (DoE) methodology in order to analyze the influence of the optical configurations on the characteristics of the fibers obtained. The experiments were carried out using a total factorial design, which means that all possible combinations of factors and levels were obtained. Two different full factorial DoEs, each one with three factors in two levels were planned. The first two factors: length of the major axis ($2\omega_{iy}$) and area of the elliptical cross section (A) of the laser beam are parameters related to the irradiance distribution of the laser beam on the filament. The third factor, *v*, is the feeding speed of the preform to the nozzle, which gives the axial velocity of the filament at the beginning of the elongation. In all experiments, the major axis of the elliptical laser beam cross section corresponds to the principal meridional plane aligned with the filament axis, and the total radiant power of the laser beam, Φ_e, is independently adjusted at each trial, progressively increasing it up to the maximum value which yields continuous fibers without filament breaking. Factors with the corresponding levels used in the first DoE1 are detailed in Table 2.

A second set of experiments was carried out with a significant reduction of the feeding rate (DoE2). In this case, a preliminary set of tests was performed in order to determine the most suitable conditions, which brought to light that the smallest diameters are obtained in the case of the shorter major axis of the laser beam. In addition, there is a tendency to decrease the diameter as the feeding speed decreases. In view of these results, a range of smaller major axes than those used in DoE1 were chosen. Table 3 shows the factors and levels of DoE2.

3. Results and discussion

3.1. Set of experiments with the BSS-1

After the set of experiments using the BSS-1 we analyzed a representative number of samples for each trial using the SEM and measured their diameters, then, the mean diameter is calculated for each trial. The processing conditions, as well as the corresponding mean diameters obtained in these trials are presented in Table 4, while Fig. 3 illustrates the typical appearance of the as produced fibers. The obtained fibers have a perfectly cylindrical shape with uniform diameter along their entire length, and all fibers show a very smooth and uniform surface with no traces of waste material (beads) or pores on their surface.

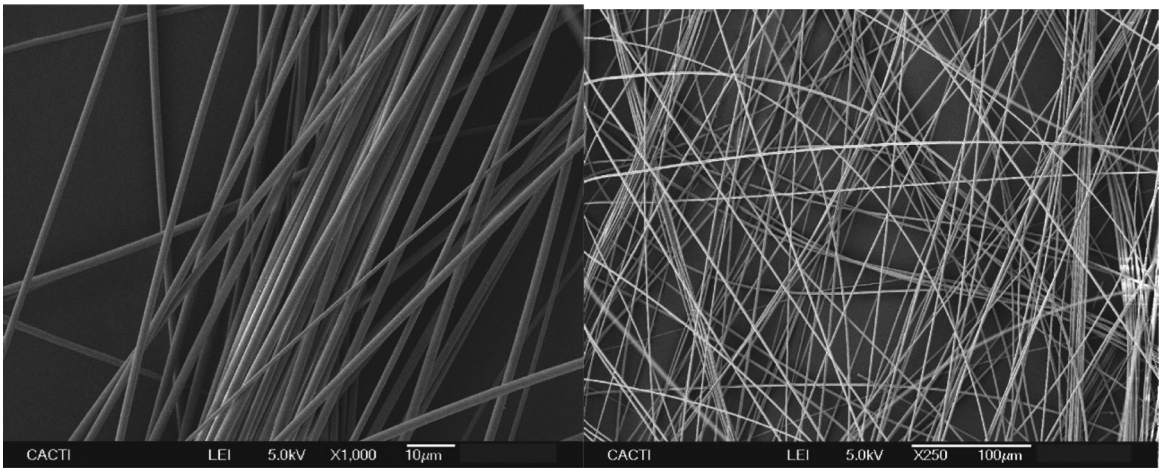

Fig. 3. SEM micrographs showing the typical appearance of the silica fibers obtained in the set of experiments performed with the BSS-1.

Table 4
Processing conditions with the corresponding mean diameters obtained by using the BSS-1. $2\omega_{is}$ is the diameter of the laser beam at the incident plane, v is the feed speed, Φ_e is the radiant flux of each laser beam, D_m is the mean diameter of the resulting fibers.

$2\omega_{is}$ (mm)	v (μm•s^{-1})	Φ_e (W)	D_m (μm)
12.4	50	800	1.57
	5	550	17.31
	5	600	10.55
	1	1750	2.38
	0.1	1750	2.31
	0.01	1750	2.14
8.2	50	288	18.61
	5	213	14.51
	5	250	10.55
	1	300	10.97
	0.1	450	3.49
	0.01	400	3.03

First, in order to analyze the effect of the radiant power, several trials were performed varying the laser power but the same feeding speed and two fixed beam diameters. With a relatively low feeding speed, 5 μm/s, and two different beam diameters of 12.4 mm and 8.2 mm, it was possible to obtain continuous fibers by using radiant powers in the ranges of 550 W to 600 W and 213 W to 250 W respectively. Noticeably, a great reduction of diameter is obtained with small increases of power; further increase of the laser power produces breakup of the molten filament, giving drops of incandescent material falling from the preform instead of a continuous fiber. On the contrary, if the power is too low, the fiber does not reach the required temperature and it is not stretched. At this point it should be noted that these results, are perfectly consistent with previous studies which support the influence of the temperature in the stability and elongation of the filament [10–12]. In this sense, an increase in the irradiance leads to higher temperature in the molten filament which corresponds to a reduction of viscosity, raising the strain rate of the elongation process which yields thinner fibers. This effect was discussed in detail and analyzed by mathematical modeling in two previous works: one for the analogous case of Laser Spinning [10], which was modeled as an uniaxial stretching flow; the second, for the present case of the Cofiblas process [12], which was modeled as an spinning process. In both cases, the temperature of the molten filament has a determining influence on the diameter obtained at the end of the process as it determines the viscosity of the molten glass. The viscosity of the fluid constitutes the main resistance to the elongational flow. Therefore, a reduced viscosity accelerates the stretching of the filament which reaches a lower diameter. However, as the laser power is further increased, the viscosity drops below the lower limit of the working window and the filament breaks forming droplets. However, this set of parameters is not suitable to produce continuous nanofibers, since the mean diameters of the fibers obtained with a feeding speed of 5 μm/s are relatively high: >10 μm.

In a different set of experiments, the feeding speed was reduced ranging from 1 μm/s to 0.01 μm/s with the same beam diameters used before. As can be clearly seen, a reduction in the feeding speed enables an increase in the maximum value of radiant power while not compromising the stability of the process. In addition, the mean diameter is reduced by reducing the feeding speed. However, the minimum diameter obtained in this case is still in the range of 2 μm to 3 μm, not reaching the nanometric range. On the other hand, the results comparing different beam diameters with the same feeding speed reveal that fibers with smaller diameter and greater homogeneity are obtained by increasing the beam diameter and the laser radiant flux. This is due to an increase in the volume where the filament maintains a suitable temperature for its elongation, corresponding to the segment between sections A and C in Fig. 1.b. At the same time, this raises the demand of radiant power since the progressive reduction of filament diameter from section A to C reduces the area exposed to the laser radiation. Notice that the diameter of the filament is in the order of several micrometers while the diameter of the beam is several millimeters. Additionally, the optical penetration depth of the laser radiation also plays another relevant role in the amount of energy absorbed by the filament. In the case of high purity fused silica for the CO_2 laser wavelength the absorption depth strongly depends on temperature. Specifically, it decays from 34 μm at 25 °C to 4 μm at 1800 °C [18]. Even though this reduction of the penetration depth favors the absorption in the thinnest sections of the filament, its minimum value is still larger than the nanometric diameter which is the basic target of this work. This constitutes another effect which drastically reduces the radiant power absorbed by the filament as its diameter decays.

It is noteworthy to mention that experiments with beam diameters smaller than 8.2 mm were also carried out. Unfortunately, it was not possible to get continuous fibers under these conditions, because it was evident that despite reducing the power to the lower limit of the laser (125 W), at such low beam diameter, the corresponding irradiance was too high to get the filament into the viscosity working window. The greater irradiance peak lead to exceeding the temperature limit, affecting the stability of the process and causing the fiber breakup. Finally, experiments with higher feeding speeds of 50 μm/s produced continuous fibers with 1.57 μm and 18.61 μm of mean diameter for the two beam diameters employed, but we couldn't find a clear correlation for these results.

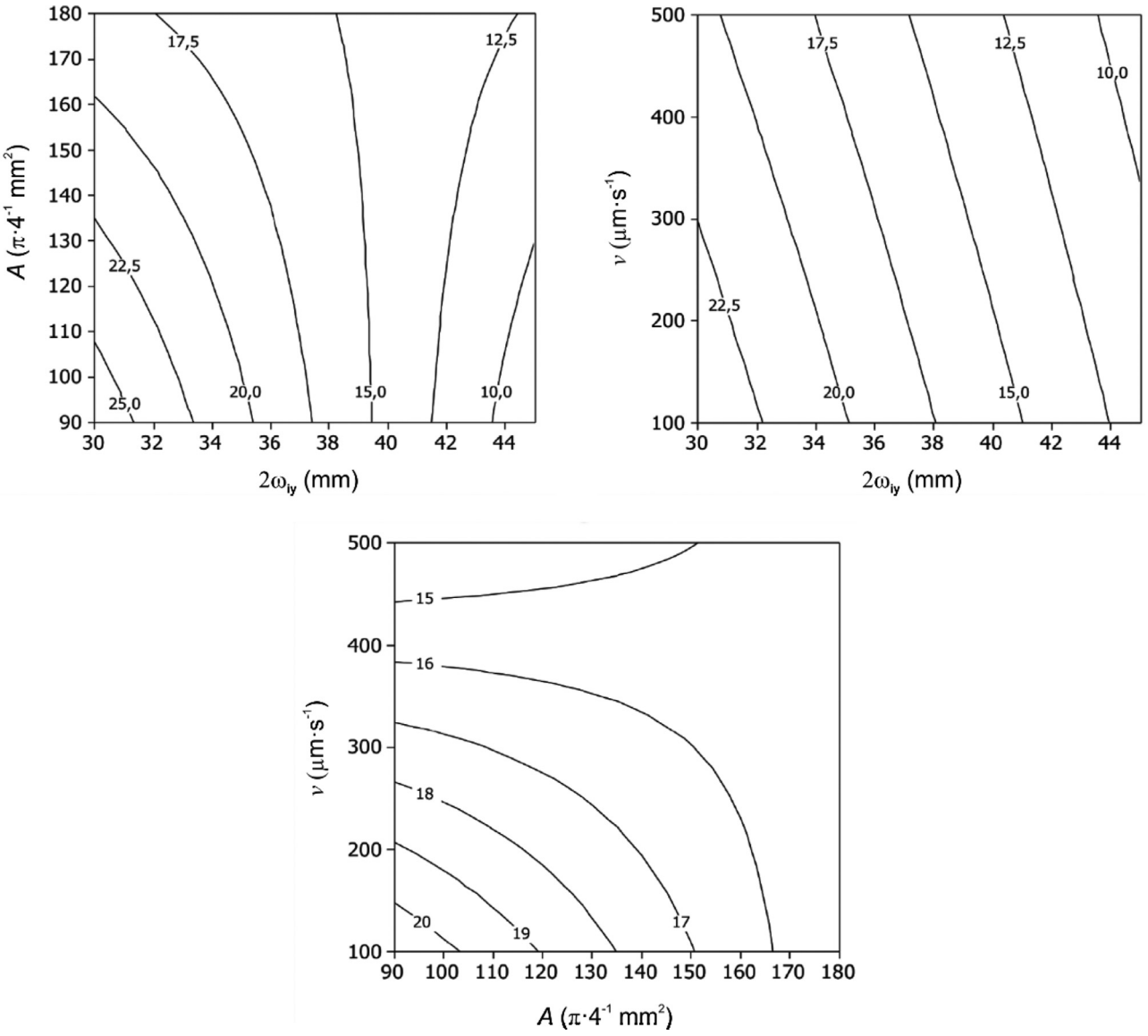

Fig. 4. Level curves of the resulting diameters of the factorial experiments made with the parameters shown in Table 5 (DoE1).

3.2. Experiments with the BSS-2: DoE1 and DoE2

The former set of experiments revealed the need for a more specific adjustment of the irradiance that would allow to lengthen the segment of the filament that is being irradiated and, at the same time, to concentrate the radiant flux in the narrow and diminishing profile of the filament. For this reason, the BSS-2 was designed and put to test in both set of experiments DoE1 and DoE2.

Table 5 details the processing conditions and resulting mean diameters for each test carried out within the framework of DoE1, including only those that ensure to obtain continuous fibers. The fibers generated have, again, a smooth cylindrical shape with uniform diameter along their entire length. Fig. 4 presents the level curves with the trend of the mean diameters as function of the factors studied. The level lines of the fiber diameters are shown in micrometers.

The analysis reveals the notable effect of the major axis of the elliptical laser beam, $2\omega_{iy}$, in this region of values of the factors studied. In particular, there is a tendency to decrease the diameter as ω_{iy} increases. The same is also observed for the feeding speed, but in this case the trend is less pronounced. Regarding the area of the laser beam at the working point, the tendency is to decrease the diameters as the area increases. This indicates that to optimize results, the differences between the irradiance applied when starting to stretch the preform and the peak irradiance should not be too pronounced, but the distance should be relatively high. The diameters of the fibers produced are still in this case higher than in the former set of experiments. The reason for this result is that this range of feeding speed was found to be too high, in relation to the maximum radiant flux available with the current laser equipment, notice that the maximum radiant power attainable by this laser (1750 W for each beam) was employed in some trials. Then, the maximum temperature reached in the filament is limited by the laser power, consequently it can't reach the lower level of viscosity in the working window required to quickly elongate the preform down to the nanometric diameter. The minimum mean diameters obtained fell slightly below 9 µm, while the maximum diameters are close to 40 µm.

In the second set of the factorial experiments, DoE2, a much lower range of feeding speeds was employed. The processing conditions and the resulting mean diameters for each test are detailed in Table 6, and the level curves of the fiber diameters in micrometers are shown in Fig. 5.

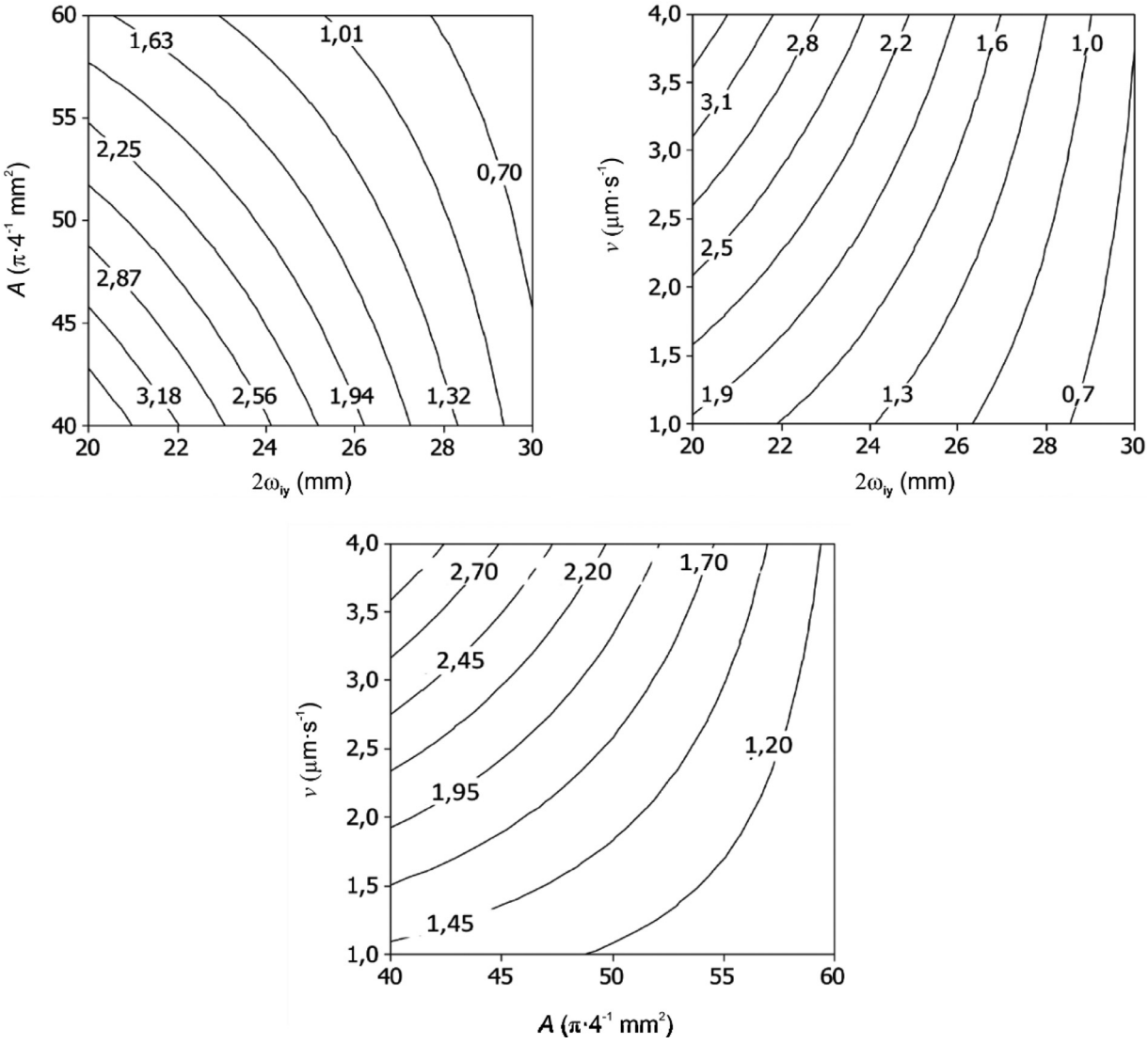

Fig. 5. Level curves of the resulting diameters (in micrometers) of the DoE2 made with the parameters shown in Table 6.

Table 5
Processing conditions with the corresponding mean diameters obtained by using the BSS-2 in DoE1. Φ_e is the radiant flux of each laser beam, v is the feed speed, $2\omega_{iy} \times 2\omega_{ix}$ is the length of the major axis times the minor axis of the laser beam at the incident plane of the preform, being A its area. D_m is the mean diameter of the resulting fibers and σ its standard deviation.

v (μm•s^{-1})	A (π•4^{-1} mm^2)	$2\omega_{iy} \times 2\omega_{ix}$ (mm^2)	Φ_e (W)	D_m (μm)	σ (μm)
100	90	30 × 3	210	34.04	4.38
100	90	45 × 2	1750	7.62	0.58
100	180	30 × 6	1000	14.69	1.38
100	180	45 × 4	1750	15.62	2.64
500	90	30 × 3	263	19.22	6.02
500	90	45 × 2	560	8.83	4.76
500	180	30 × 6	370	21.98	2.38
500	180	45 × 4	1750	8.93	1.94

Again, the level curves reveal a significant influence of the major axis of the elliptical laser beam, $2\omega_{iy}$, and its area on the diameter of the fibers. Both effects are related with the length of the segment of material irradiated and the progressive change of irradiance along it, in the same way as explained in the previous paragraphs. As the major axis of the cross section is increased the laser beam reaches a longer segment of the preform with a proper level of irradiance, the filament keeps the suitable viscosity for stretching along a longer length and, consequently, the elongation continues down to a lower diameter. On the contrary, an increase in speed has the opposite effect. The best results were obtained with high radiant power (1750 W) and low feeding speed (1 μm/s), leading to obtain fibers with the smallest mean diameter (0.37 μm). The

Table 6
Processing conditions with the corresponding mean diameters obtained by using the BSS-2 in DoE2. Φ_e is the radiant flux of each laser beam, v is the feed speed, $2\omega_{iy} \times 2\omega_{ix}$ is the length of the major axis times the minor axis of the laser beam at the incident plane of the preform, being A its area. D_m is the mean diameter of the resulting fibers and σ its standard deviation.

v (μm•s^{-1})	A (π•4^{-1} mm^2)	$2\omega_{iy} \times 2\omega_{ix}$ (mm^2)	Φ_e (W)	D_m (μm)	σ (μm)
1	40	20 × 2	275	2.05	0.64
1	60	20 × 3	450	1.40	0.52
1	40	30 × 1.3	1750	0.62	0.17
1	60	30 × 2	1750	0.37	0.08
4	40	20 × 2	225	5.68	2.05
4	60	20 × 3	400	1.91	0.44
4	40	30 × 1.3	1750	1.00	0.47
4	60	30 × 2	1750	0.49	0.1

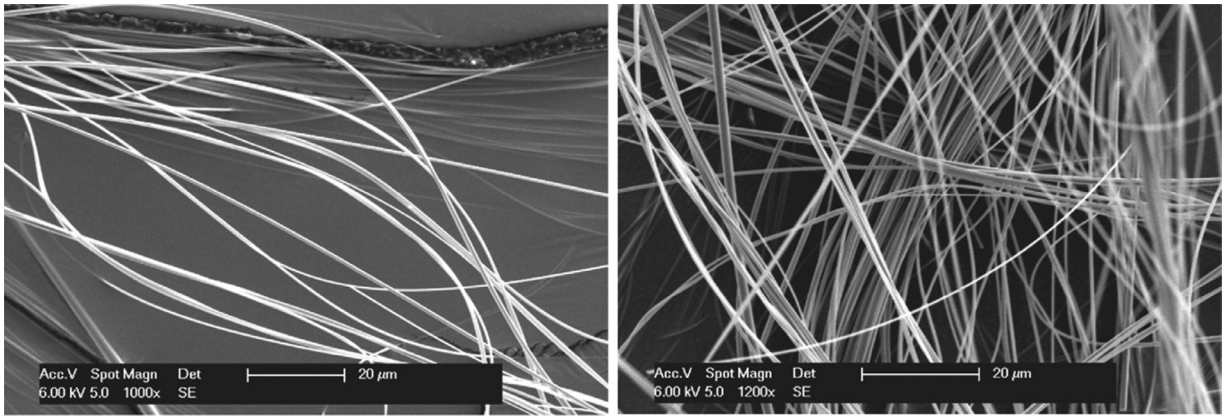

Fig. 6. SEM micrographs of the silica fibers obtained in the second set of experiments performed with the BSS-2, DoE2, presenting mean diameters of: (a) 0.62 μm, (b) 0.37 μm.

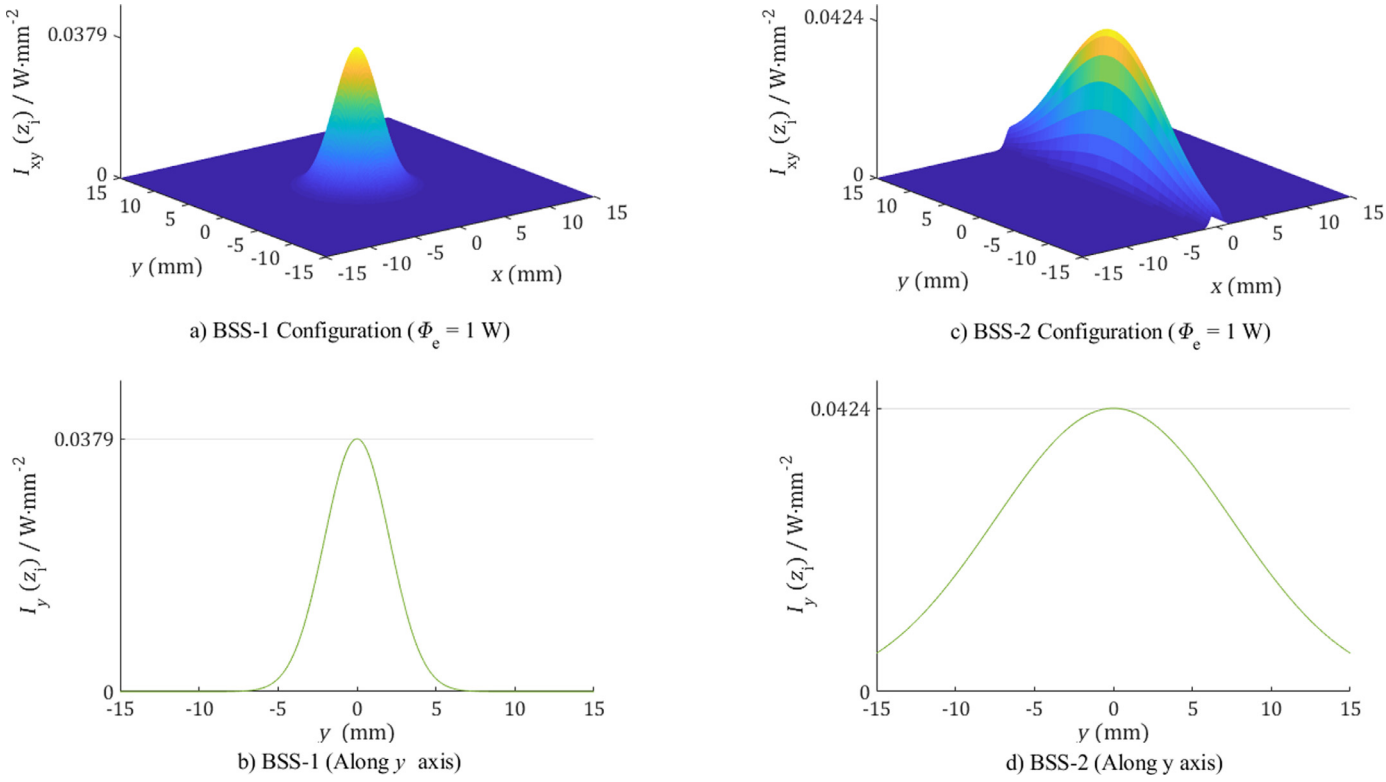

Fig. 7. Comparison of irradiance distribution obtained at the incident plane (z_i) using the BSS-1 and BSS-2 with total radiant flux normalized to 1 W. (a) and (c) represent the two-dimensional irradiance distribution at the laser beam cross section, (b) and (d) show the irradiance distribution along the y axis.

diameters obtained in this set of experiments are one order of magnitude smaller than those obtained previously in DoE1, which reflects the enormous influence of the speed. Moreover, the results obtained in this case bring to light the effectiveness of this anamorphic beam-shaping system compared to the BSS-1 composed of spherical lenses. An example of the fibers obtained in these experiments is presented in Fig. 6, showing fibers with a regular cylindrical shape, uniform diameter along their entire length, and a very smooth surface.

Therefore, results of the set of experiments DoE1 and DoE2 led to the same trends even though they produce fibers of different diameters. On one hand, by decreasing the feeding speed, the fibers produced have smaller diameters. On the other hand, by increasing the length of the segment irradiated by the laser beam with a higher irradiance level, also implies an improvement of the diameters. These results, bring to light the improvement that involves the implementation of the BSS-2 based on the combination of spherical and cylindrical lenses to obtain a suitable irradiance distribution. This combination allowed to increase the irradiance along the axis in the direction of the preform (*y*-axis / major axis), while the width of the laser beam at the incident plane (*x*-axis / minor axis) can be reduced independently to adjust it to the filament diameter.

Fig. 7 shows a comparison of the irradiance distribution at the incident plane obtained using both BSS-1 and BSS-2. For this aim, the two-dimensional irradiance distribution and the irradiance along the y axis were plotted using Eq. (1). The beam irradiance at the center of the beam, $I_0(z)$, was estimated, according to Eq. (2), in both cases for the same total radiant flux of 1 W for easy comparison. As we explained previously, both optical systems provide a Gaussian irradiance distribution with circular section in the case of BSS-1 and elliptical for the BSS-2. However, another important difference is that the BSS-2 yields a higher peak of irradiance, and it remains at high values a longer distance from the center along the *y* axis. This distribution provides a high level of irradiance at the point where the filament begins to stretch (point A in Fig. 1.b) and, at the same time, the maximum is reached at a distance sufficiently far from the start to coincide with a notable reduction in the diameter of the filament (point B in Fig. 1.b). In this way, the elongation of the filament is extended until the diameter and irradiance are already markedly reduced (point C, Fig. 1.b), what makes it possible to obtain finer fibers. This effect was observed experimentally and analyzed using mathematical modeling in our previous publication [12].

4. Conclusions

In this paper, a simple design of an anamorphic beam shaping system was effectively implemented to convert the circular Gaussian beam profile of a high power CO_2 laser into an elliptical Gaussian profile with orthogonal astigmatism, where the irradiance distribution can be independently adjusted in the two principal meridional planes. The efficacy and usefulness of this beam-shaping system in a specific case was experimentally demonstrated through an extensive series of glass nanofiber production experiments using the Cofiblas technique. Even though the optical system with spherical lenses was proved to be suitable to obtain continuous fibers of small diameter at a relative high rate of production, only the use of the anamorphic beam shaping system succeeded to produce sub-micrometer diameters, thanks to the specifically shaped irradiance distribution. This simple anamorphic beam shaping system allowed to concentrate the radiant power of the laser beam along the axis of the preform, and to obtain a high level of irradiance on the filament. As a result, the anamorphic beam shaping system makes possible a reduction of 84.5 % in the diameter compared to the optical system with spherical lenses under the same processing conditions (laser radiant power and preform feeding speed).

Declaration of Competing Interest

The authors declare the following financial interests/personal relationships which may be considered as potential competing interests

Acknowledgements

We acknowledge the help of A. Abalde with the construction of the experimental system. Technical staff of CACTI at University of Vigo is also acknowledged by their help with the characterization of some samples.

Funding

This work was partially supported by the EU research project Bluehuman (EAPA_151/2016 Interreg Atlantic Area), Government of Spain [PGC2018–094900-B-I00 (MCIU/AEI/FEDER, UE)], and by Xunta de Galicia (ED431C 2019/23).

References

[1] Dzenis Y. Structural nanocomposites. Science 2008;319(80-):419–20. doi:10.1126/science.1151434.
[2] Ritchie RO. The conflicts between strength and toughness. Nat Mater 2011;10:817–22. doi:10.1038/nmat3115.
[3] Griffith AA, Taylor GI. The phenomena of rupture and flow in solids. Philos Trans R Soc London Ser A, Contain Pap a Math or Phys Char 1921;221:163–98. doi:10.1098/rsta.1921.0006.
[4] Peng K, Nain A, Mirzaeifar R. Tracking the origins of size dependency in the mechanical properties of polymeric nanofibers at the atomistic scale. Polymer (Guildf) 2019;175:118–28. doi:10.1016/j.polymer.2019.05.014.
[5] Erden S, Ho K. 3 - Fiber reinforced composites. In: Fiber technol. fiber-reinforced compos. Woodhead Publishing; 2017. p. 51–79. https://doi.org/https://doi.org/. doi:10.1016/B978-0-08-101871-2.00003-5.
[6] Hausrath RL, Longobardo AV. High-strength glass fibers and markets. editors. Fiberglass glas. technol. energy-friendly compos. appl. 2010:197–228. doi:10.1007/978-1-4419-0736-3.
[7] Luo J, Wang J, Bitzek E, Huang JY, Zheng H, Tong L, et al. Size-dependent brittle-to-ductile transition in silica glass nanofibers. Nano Lett 2016;16:105–13. doi:10.1021/acs.nanolett.5b03070.
[8] Wallenberger FT, Bingham PA. Fiberglass and glass technology: energy-friendly compositions and applications. Springer; 2010. doi:101007/978-1-4419-0736-3.
[9] Quintero F, Mann AB, Pou J, Lusquiños F, Riveiro A. Rapid production of ultralong amorphous ceramic nanofibers by laser spinning. Appl Phys Lett 2007;90:153109. doi:10.1063/1.2722202.
[10] Quintero F, Dieste O, Pou J, Lusquiños F, Riveiro A. On the conditions to produce micro- and nanofibres by laser spinning. J Phys D Appl Phys 2009;42:065501. doi:10.1088/0022-3727/42/6/065501.
[11] Quintero F, Dieste Ó, Penide J, Lusquiños F, Riveiro A, Pou J. Nonconventional production of glass nanofibers by laser spinning. J Am Ceram Soc 2014;97:3116–21. doi:10.1111/jace.13127.
[12] Quintero F, Penide J, Riveiro A, del Val J, Comesaña R, Lusquiños F, et al. Continuous fiberizing by laser melting (Cofiblas): production of highly flexible glass nanofibers with effectively unlimited length. Sci Adv 2020;6:eaax7210. doi:10.1126/sciadv.aax7210.
[13] Zhang J, Chen X, Li F, Liu H, Sun X, Ma M. Paraxial lens design of anamorphic lenses with a fixed anamorphic ratio. OSA Contin 2019;2:1430–54. doi:10.1364/OSAC.2.001430.
[14] Kumstel J. Laser polishing of metallic freeform surfaces by using a dynamic laser beam preforming system. J Laser Appl 2021;33:22020. doi:10.2351/1.5128459.
[15] Yariv A. Quantum electronics. 3rd ed. New York; 1989.
[16] Self SA. Focusing of spherical Gaussian beams. Appl Opt 1983;22:658–61. doi:10.1364/AO.22.000658.
[17] Siegman AE. Analysis of laser beam quality degradation caused by quartic phase aberrations. Appl Opt 1993;32:5893–901. doi:10.1364/AO.32.005893.
[18] McLachlan AD, Meyer FP. Temperature dependence of the extinction coefficient of fused silica for CO_2 laser wavelengths. Appl Opt 1987;26:1728. doi:10.1364/ao.26.001728.